

Cluster Ion Thermal Decomposition (II): Master Equation Modeling in the Low-Pressure Limit and Fall-Off Regions. Bond Energies for $\text{HSO}_4^-(\text{H}_2\text{SO}_4)_x(\text{HNO}_3)_y$

Edward R. Lovejoy* and Joachim Curtius†

NOAA Aeronomy Laboratory, 325 Broadway, Boulder, Colorado 80305

Received: July 2, 2001; In Final Form: September 26, 2001

The thermal decomposition kinetics of a wide range of cluster ions in and near the low-pressure limit were modeled with a master equation analysis based on an exponential up energy transfer model and an orbiting transition state. Cluster ion bond energies and helium-cluster ion energy transfer parameters were derived. Analysis of the temperature and pressure dependent decomposition kinetics of a set of clusters, for which bond enthalpies have been measured, showed that the master equation approach reproduces the literature bond energies to better than 1 kcal mol⁻¹. The helium-cluster ion energy transfer was found to be very efficient, resembling the predictions of ergodic collision theory. On the basis of the results of the modeling of the calibration clusters, the analysis was extended to derive bond energies for the important atmospheric cluster ions of the form $\text{HSO}_4^-(\text{H}_2\text{SO}_4)_x(\text{HNO}_3)_y$, ((*x*, *y*) = (1–5, 0), (0, 1–2), and (1, 1)).

Introduction

This paper describes master equation modeling of the kinetics of thermal decomposition of cluster ions. The primary goals of this work were to develop a methodology for deriving bond energies from measurements of the kinetics of decomposition as a function of pressure and temperature, and to improve the understanding of intermolecular energy transfer and unimolecular decomposition processes of cluster ions. There is considerable interest in the fundamental processes of intermolecular energy transfer and unimolecular decomposition due to their critical roles in chemical reactions.^{1–6}

In a recent paper,⁷ the analysis of the thermal decomposition kinetics of cluster ions measured in a quadrupole ion trap in the low-pressure limit was described. It is shown that the cluster ion bond energies E_o are related to the low-pressure limit decomposition activation energy E_a by the simple relation: $E_o = E_a + U_{\text{vib}} + 1.2k_B T$, where U_{vib} is the average vibrational energy of the reactant at the mean temperature T , and k_B is the Boltzmann constant. This expression is consistent with Tolman's theorem⁸ that states that the activation energy for a reaction is the difference between the rate weighted average energy of the reacting molecules ($E_o - 1.2k_B T$) and the average energy of the whole population U_{vib} . The average energy of the reacting molecules is slightly less than the threshold energy because collisions that take molecules above the threshold energy are essentially reactive due to the efficient unimolecular decomposition at all energies above threshold.

The present paper describes the master equation modeling of the decomposition kinetics of the cluster ions analyzed in previous work,⁷ as well as for cluster ions of the form $\text{HSO}_4^-(\text{H}_2\text{SO}_4)_x(\text{HNO}_3)_y$ described in the preceding paper.⁹ The kinetics of the larger clusters $\text{HSO}_4^-(\text{H}_2\text{SO}_4)_{3,4,5}$ are in the fall-off region and the simple relationship between bond energy and activation energy derived for the smaller cluster ions in the low-

pressure limit is not valid. A master equation analysis based on an exponential up energy transfer model and an orbiting transition state fits the thermal decomposition kinetics of the cluster ions, and literature bond energies are reproduced to within about 1 kcal mol⁻¹. The master equation modeling shows that the He-cluster ion energy transfer is efficient and resembles predictions of ergodic collision theory.

Experimental Section

The experimental apparatus and procedures used in the present work were the same as described in the preceding paper,⁹ and are not discussed here.

Master Equation Modeling. The discrete master equation describing thermal decomposition is given by^{4,10}

$$\frac{d[i]}{dt} = z[M] \sum_{j=1}^{\infty} P_{ij}[j] - z[M][i] \sum_{j=1}^{\infty} P_{ji} - k_{\text{uni},i}[i] \quad (1)$$

where z is the second-order collision rate constant for bath gas (M) + reactant, P_{ij} is the probability that a collision between the reactant and the bath gas changes the internal energy of the reactant from state j to state i , and $k_{\text{uni},i}$ is the first-order unimolecular decomposition rate constant of state i . The collision rate coefficient z was assumed to be independent of the reactant state and was calculated with the Langevin expression based on an ion–ion induced dipole interaction appropriate for the He bath gas.¹¹ The first term on the right-hand side of eq 1 accounts for the increase in the population of state i due to collisions with the bath gas that convert the other states j into state i . The second term describes the loss of population in state i due to collisions that convert state i into the other states. The last term is the unimolecular decomposition of state i leading to products. In the present work, the energy level structure of the cluster ion was approximated by $n = 100$ to 200 equally spaced levels extending from the zero point energy of the reactant to 1.4–2.5 times the bond energy, giving energy level spacing ranging from 0.1 to 0.5 kcal mol⁻¹. The set of n differential equations described by eq 1 was integrated numerically with routines optimized for stiff sets of equations.¹²

* To whom correspondence should be addressed. E-mail: edward.r.lovejoy@al.noaa.gov.

† Also affiliated with the Cooperative Institute for Research in Environmental Studies, University of Colorado, Boulder, Colorado.

A variety of functions have been used to parametrize the energy transfer probabilities $P_{j,i}$.¹³ Experimental and theoretical studies suggest that, at least for neutral systems, the energy transfer between the bath gas and the reactant is well described by an exponential model.¹⁴ In the present work, the probability of energy transfer from state i to j , $P_{j,i}$, was modeled with an exponential up function

$$P_{j,i} = C_i \exp\left(\frac{-(E_j - E_i)}{\beta}\right) \quad j \geq i \quad (2)$$

where E_i is the energy of state i , and β is the average energy transferred in up collisions. Up collisions result in an increase in the internal energy of the reactant. The choice of an exponential up model as opposed to an exponential down model is rationalized in the discussion section. The down probabilities are given by detailed balance

$$P_{j,i} = P_{i,j} \frac{\rho(E_j) \exp\left(\frac{-E_j}{k_B T}\right)}{\rho(E_i) \exp\left(\frac{-E_i}{k_B T}\right)} \quad j < i \quad (3)$$

where $\rho(E)$ is the density of states of the reactant at energy E . The coefficients C_i are determined by the normalization condition

$$\sum_{j=1}^{\infty} P_{j,i} = 1 \quad (4)$$

A single normalization coefficient was used for all of the levels. The normalization factor was chosen to properly normalize the probabilities at the reaction threshold. The normalization scheme described by Gilbert and King¹⁵ was not used, because it produced negative coefficients (C_i) at the higher energies for the conditions of the present calculations (see e.g., ref 4). The normalization procedure employed in the present calculations is not strictly correct because eq 4 is not satisfied for all levels. However, the largest deviations occur at low and high energies well away from the threshold energy where they do not significantly influence the kinetics. The states at low energy maintain a Boltzmann distribution during the reaction and do not contribute significantly to the overall kinetics because they are far below threshold. The states well above threshold have negligible population at steady state, particularly in the low-pressure limit, and do not contribute significantly to the reactive flux.

The average energy transferred up and down per collision at energy E_i are given by the following expressions

$$\langle E \rangle_{i,up} = \frac{\sum_{j=i+1}^{\infty} P_{j,i} (E_j - E_i)}{\sum_{j=i+1}^{\infty} P_{j,i}} \quad (5)$$

and

$$\langle E \rangle_{i,down} = \frac{\sum_{j=1}^{i-1} P_{j,i} (E_i - E_j)}{\sum_{j=1}^{i-1} P_{j,i}} \quad (6)$$

The net average energy transferred is given by

$$\langle E \rangle_{i,net} = \frac{\sum_{j=1}^{\infty} P_{j,i} (E_j - E_i)}{\sum_{j=1}^{\infty} P_{j,i}} \quad (7)$$

Unimolecular decomposition rate coefficients k_{uni} were calculated by using the RRKM expression

$$k_{uni}(E, J) = \frac{sN(E, J)}{\hbar \rho(E, J)} \quad (8)$$

where s is the reaction symmetry factor, $N(E, J)$ is the number of open reaction channels at the transition state for a total energy E and angular momentum J , and $\rho(E, J)$ is the density of states of the reactant ion. Averaging over the J distribution of the reactant yields $k_{uni}(E)$. The number of open reaction channels $N(E, J)$ were calculated by using an orbiting transition state as described by Chesnavich and Bowers.¹⁶ The orbiting transition state is located at the maximum of the long-range effective potential. The semiclassical angular momentum state counts presented by Chesnavich and Bowers¹⁶ were used with the interpolation scheme given by Olzmann and Troe.¹⁷ For all of the decomposition reactions, except $\text{Cl}^- \text{H}_2\text{O} \rightarrow \text{Cl}^- + \text{H}_2\text{O}$, it was assumed that both products are spherical tops and the geometric average rotational constants were used ($B_s = (ABC)^{1/3}$). Chesnavich and Bowers¹⁸ have shown that the errors associated with this assumption are small. For the $\text{Cl}^- \text{H}_2\text{O}$ reaction, the atom-sphere expressions were employed. All of the reactant ions were treated as spherical tops and geometric mean rotational constants were used. The semiclassical angular momentum state counts of Chesnavich and Bowers¹⁸ are based on an ion-ion induced dipole potential. However, all of the neutral reaction products in the present study have permanent dipole moments. Following Bass and Bowers,¹⁹ the polarizabilities of the neutral products were scaled so that the Langevin ion-ion induced dipole rate constant equaled Su and Chesnavich's ion-polar molecule rate constant.²⁰ Most of the neutral product dipole moments and polarizabilities were taken from standard sources.²¹ The sulfuric acid dipole moment (2.73 D) is from the microwave spectroscopic study of Kuczkowski et al.,²² and the H_2SO_4 and HNO_3 polarizabilities (5.4 and 3.8 Å³, respectively) are from Lippincott et al.²³

Reactant and product vibrational states were counted using the Beyer-Swinehart algorithm²⁴ with an energy grid size typically at least 5 times smaller than the lowest vibrational frequency. Vibrational frequencies were calculated ab initio at the HF/6-31+G(d) level and scaled by a factor of 0.89.²⁵ Details of the ab initio calculations are presented elsewhere.^{7,9}

The experimental kinetics were modeled with the master equation formalism described above. Input to the model includes the reactant and product vibrational frequencies and rotational constants, the bond energy, and the average energy transfer parameter β . The master equation was integrated for reaction times up to 10 s, comparable to the experimental reaction times.

TABLE 1: Best-Fit Master Equation Bond Energies and Energy Transfer Parameters for the Calibration Clusters

reaction	E_o lit. ^a (kcal mol ⁻¹)	T ^b (K)	β ^c (kcal mol ⁻¹)	E_o ^c (kcal mol ⁻¹)	ΔH°_{298K} (kcal mol ⁻¹)
$H^+(H_2O)_4 \rightarrow H^+(H_2O)_3 + H_2O$	17.1	342	1.13	17.1	17.3
$H^+(H_2O)_3 \rightarrow H^+(H_2O)_2 + H_2O$	20.4	430	1.22	19.8	20.2
$H^+(CH_3OH)_3 \rightarrow H^+(CH_3OH)_2 + CH_3OH$	22.8	358	1.60	21.9	21.6
$H^+(C_2H_5OH)_2 \rightarrow H^+C_2H_5OH + C_2H_5OH$	32.4	506	1.80	31.4	31.3
$H^+(CH_3CN)_2 \rightarrow H^+CH_3CN + CH_3CN$	31.4	540	1.55	29.5	29.2
$H^+((CH_3)_2CO)_2 \rightarrow H^+(CH_3)_2CO + (CH_3)_2CO$		488	1.70	31.7	31.3
$NO_3^-(HNO_3)_2 \rightarrow NO_3^-HNO_3 + HNO_3$	18.0	346	1.20	19.4	18.9
$Cl^-H_2O \rightarrow Cl^- + H_2O$	12.6	439	1.40	11.0	12.6

^a Average literature value (refs 7 and 46). ^b Median reaction temperature. ^c Optimized master equation modeling parameters for an exponential up model with average energy up = β , and bond energy = E_o .

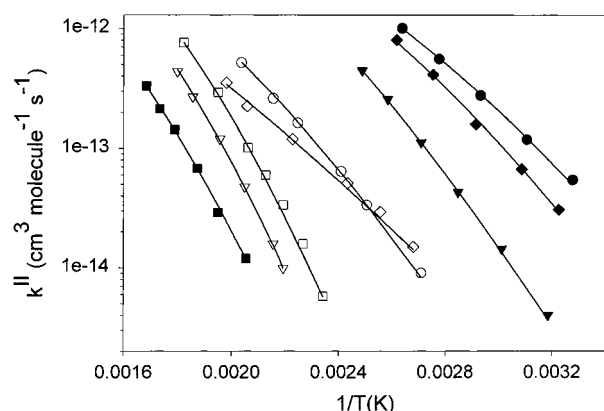


Figure 1. Arrhenius plots for the calibration clusters. Solid lines are master equation results using parameters listed in Table 1. Symbols are as follows: solid circles = $H^+(H_2O)_4$, open circles = $H^+(H_2O)_3$, solid triangles = $H^+(CH_3OH)_3$, open triangles = $H^+(C_2H_5OH)_2$, solid squares = $H^+(CH_3CN)_2$, open squares = $H^+((CH_3)_2CO)_2$, solid diamonds = $NO_3^-(HNO_3)_2$, and open diamonds = Cl^-H_2O .

The cluster ion decomposition kinetics rapidly reached a steady-state characterized by a single-exponential decay. The experimental kinetics were fit with a manual iterative scheme that involved varying the bond energy and the energy transfer parameter to a precision of less than 0.1 kcal mol⁻¹.

Results and Discussion

Master Equation Calculations for the Calibration Clusters. Master equation calculations were performed for the decomposition reactions of the 8 cluster ions examined in the previous study⁷ (Table 1). These cluster ions are referred to collectively as the “calibration” clusters in the present work since there are previous measurements of their bond enthalpies. All of the calibration ions had decomposition kinetics in or near the low-pressure limit. In the low-pressure limit the unimolecular decomposition (k_{uni}) of the reactant is much faster than the bath gas–reactant energy transfer ($z[He]$), and the overall decomposition kinetics are sensitive mostly to the reaction threshold energy and the efficiency of the energy transfer.

The temperature dependencies of the calibration cluster second order decomposition rate coefficients and the master equation modeled results are plotted in Figure 1. The subtle curvature in the temperature dependence of the decomposition rate constants is reproduced by the calculations. The absolute

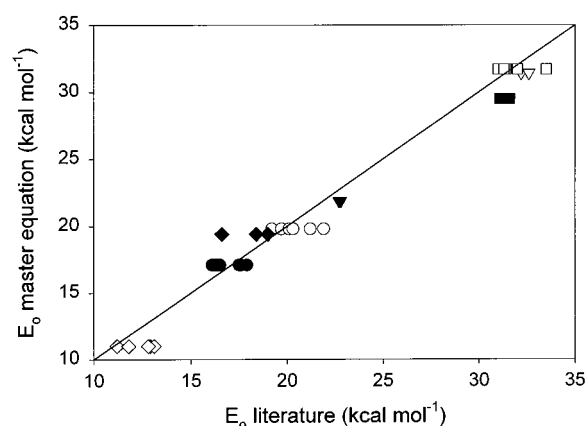


Figure 2. Comparison of master equation derived bond energies and the literature bond energies. The literature bond energies were derived from the experimental bond enthalpies listed in ref 46.

magnitudes and temperature variation are reproduced with the model by using bond energies typically within 1 kcal mol⁻¹ of the literature values and with average energies up between about 1 and 2 kcal mol⁻¹. The bond energies E_o and average energies up β are listed in Table 1. The derived bond energies are plotted vs the literature values in Figure 2. The average absolute deviation ($|E_o(\text{literature}) - E_o(\text{master equation})|$) is 0.9 kcal mol⁻¹ and the average deviation ($E_o(\text{literature}) - E_o(\text{master equation})$) is 0.6 kcal mol⁻¹.

The agreement between derived bond energies and literature values was much poorer when a constant average energy down model was applied. The best fit bond energies for the fixed average energy down model were systematically about 2 kcal mol⁻¹ lower than the literature values, suggesting that the average energy down model does not accurately describe the energy transfer. This is consistent with the consensus that the average energy transfer for highly excited molecules decreases with decreasing internal energy.^{14,26} In recent detailed studies of the energy transfer of highly excited aromatic compounds, Luther and co-workers²⁷ find that the energy transfer is well described by an exponential model with an average energy down that decreases approximately linearly with decreasing internal energy. The following discussion shows that the exponential model described by Luther and co-workers is similar to the exponential constant average energy up model used in the present study.

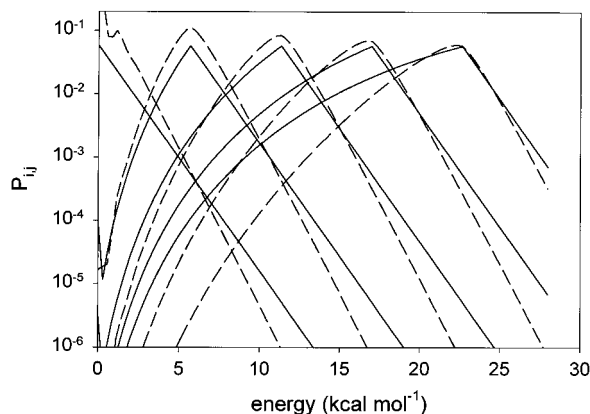


Figure 3. $\text{H}^+(\text{H}_2\text{O})_3$ energy transfer probabilities for the exponential up model ($\beta = 1.22 \text{ kcal mol}^{-1}$ and $E_0 = 19.8 \text{ kcal mol}^{-1}$, solid lines) and for ergodic collision theory (dashed lines) at 445 K. The energy level spacing is $0.28 \text{ kcal mol}^{-1}$.

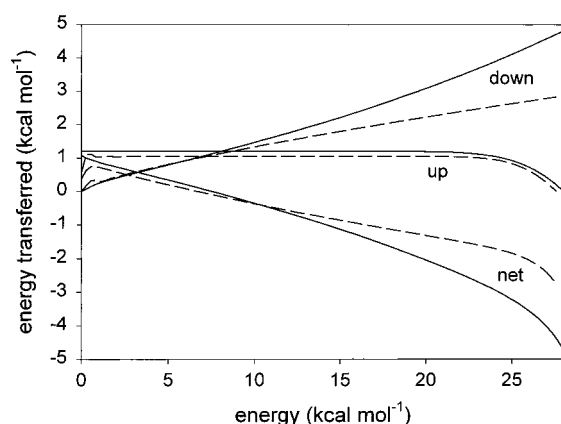


Figure 4. Calculated average $\text{H}^+(\text{H}_2\text{O})_3$ energy transfer for the energy transfer probabilities shown in Figure 3 for the exponential up model (solid lines) and ergodic collision theory (dashed lines).

Energy transfer probabilities for $\text{H}^+(\text{H}_2\text{O})_3$ calculated with the exponential up model and optimized master equation parameters (Table 1) are shown in Figure 3. The corresponding average energies transferred (net, up, and down) are plotted in Figure 4. It is apparent that for the exponential up model, the net average energy transferred and the average energy transferred down are approximately linear functions of energy with slight curvature, similar to the general conclusions from direct energy transfer studies by Luther and co-workers.²⁷ The roll-over at the highest energies is due to the fact that energy transfer is not allowed to populate states above about 28 kcal mol^{-1} , the highest energy considered in the model.

The exponential up model is consistent with physical insight. The source of the energy for the upward transitions is the relative collision energy. The relative collision energy is a function of the bath temperature and not a function of the internal energy of the reactant molecule. Therefore, it is reasonable that the average energy up is approximately independent of the internal energy of the reactant. Conversely, in downward transitions, energy is transferred from the reactant to the bath gas, and it is likely that reactants with higher internal energy transfer more energy to the bath gas per collision. In the present work, the exponential average energy up model was employed because it is physically realistic, it has only one parameter (β), and it fits the data.

The previous measurements⁷ of the variation of the $\text{H}^+(\text{H}_2\text{O})_3$ first-order decomposition rate coefficients as a function of He concentration are shown in Figure 5. The master equation model

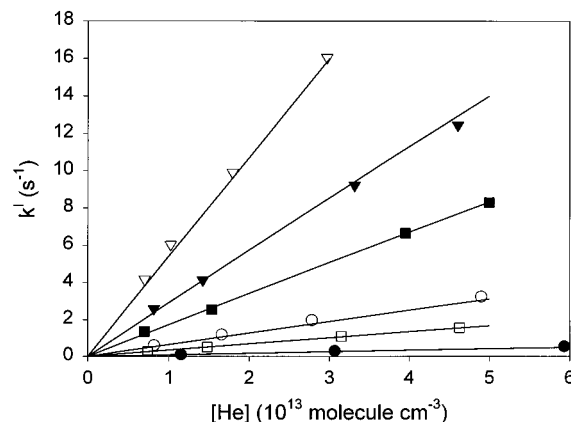


Figure 5. Pressure dependence of the first-order rate coefficient for $\text{H}^+(\text{H}_2\text{O})_3$ decomposition as a function of temperature. The temperatures are 369, 399, 415, 445, 464, and 491 K. Symbols are experimental data from ref 7. The solid lines are master equation calculations with $E_0 = 19.8 \text{ kcal mol}^{-1}$ and $\beta = 1.22 \text{ kcal mol}^{-1}$.

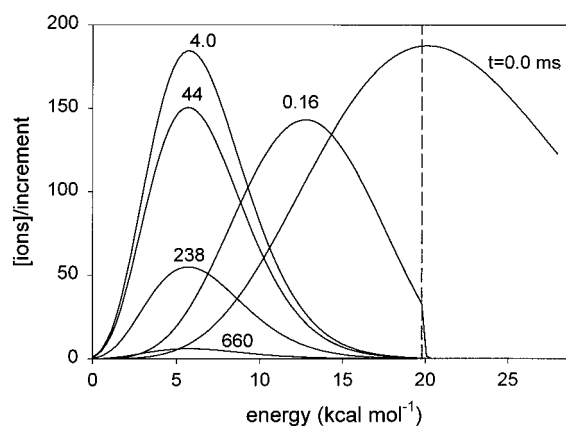


Figure 6. Calculated $\text{H}^+(\text{H}_2\text{O})_3$ internal energy distributions as a function of time. Reaction times are indicated above the curves. The initial conditions are a 1000 K Boltzmann distribution with 10^4 ions. The dashed vertical line marks the reaction threshold. The energy level spacing is $0.28 \text{ kcal mol}^{-1}$. The conditions are $T = 445 \text{ K}$, $E_0 = 19.8 \text{ kcal mol}^{-1}$, $\beta = 1.22 \text{ kcal mol}^{-1}$, and $[\text{He}] = 3 \times 10^{13} \text{ molecule cm}^{-3}$.

(solid lines), based on exponential up energy transfer, reproduces both the pressure and temperature variations. The calculated populations of energy states for $\text{H}^+(\text{H}_2\text{O})_3$ as a function of time are shown in Figure 6 for the optimized average energy up β and bond energy E_0 , at 445 K and $[\text{He}] = 3 \times 10^{13} \text{ molecule cm}^{-3}$. The unimolecular decomposition rate coefficients $k_{\text{uni}}(E)$ for the same conditions are plotted in Figure 7. A 1000 K Boltzmann distribution was chosen as the starting point for the $\text{H}^+(\text{H}_2\text{O})_3$ master equation calculations to crudely account for heating of the ions during the trapping process. Ions are drawn into the trap with small potentials ($< 5 \text{ V}$), and the resulting kinetic energy must be dissipated to achieve trapping. The energy is dissipated in collisions that lead initially to an increase in the internal energy of the trapped ions. The master equation calculations show that the initial energy distribution does influence the rapid transient relaxation, but this transient decays on a time scale that is typically much shorter than the time scale of the thermal decomposition.

The $\text{H}^+(\text{H}_2\text{O})_3$ unimolecular decomposition rate coefficients (k_{uni}) are much larger than the energy transfer rate constants, even close to threshold. This makes the decomposition kinetics sensitive mainly to the rate of energy transfer, which is dependent on the bath gas pressure, and leads to low-pressure-limit behavior. The large decomposition rate coefficients at

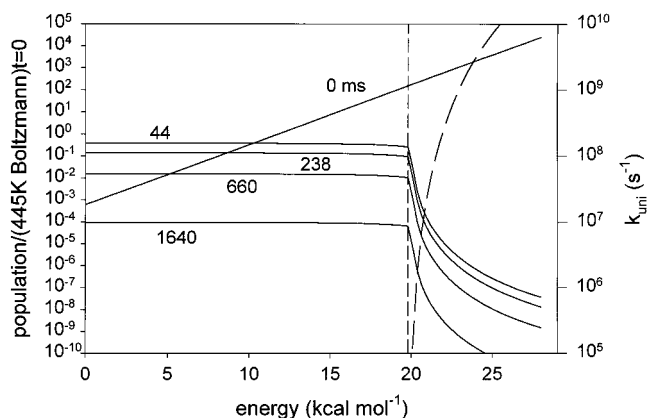


Figure 7. Calculated $\text{H}^+(\text{H}_2\text{O})_3$ energy distributions and unimolecular decomposition rate constants. The solid lines are the energy distributions plotted as the ratio to a 445 K Boltzmann distribution at $t = 0$. The dashed vertical line marks the reaction threshold. The dashed curve is $k_{\text{uni}}(E)$. Conditions and data are the same as in Figure 6.

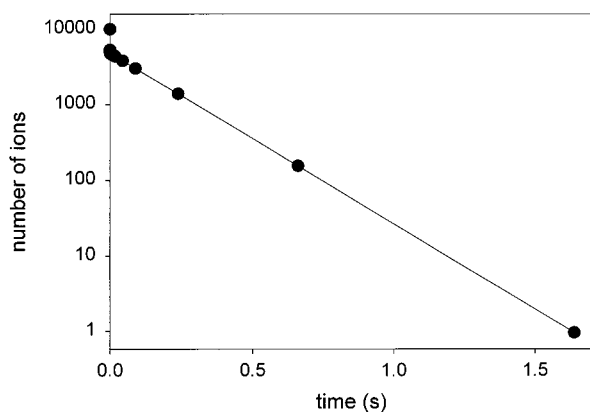


Figure 8. Calculated temporal variation of the number of $\text{H}^+(\text{H}_2\text{O})_3$ ions for the same conditions as in Figure 6. The line is an exponential fit for $t > 0.005$ s.

threshold are mostly a result of the relatively low density of states of $\text{H}^+(\text{H}_2\text{O})_3$ (1.8×10^{10} states $\text{kcal}^{-1} \text{mol}$ at $E_0 = 19.8$ kcal mol^{-1} and $(\hbar\rho(E_0))^{-1} = 580$ s^{-1}). The first-order ion-He collision rate coefficients ($z[\text{He}]$) are about 2×10^4 s^{-1} for $[\text{He}] = 3 \times 10^{13}$ molecule cm^{-3} . In less than 4 ms the initial $\text{H}^+(\text{H}_2\text{O})_3$ 1000 K distribution evolves to resemble the ambient 445 K distribution, that then decays exponentially (Figure 8) due to decomposition. The shift from the initial 1000 K distribution to the steady state approximate 445 K distribution is accompanied by a significant decrease in ion concentration due to very rapid decomposition of ions with energies initially above the threshold. The energy level populations are plotted as the ratio to a 445 K equilibrium population at $t = 0$ in Figure 7. This figure clearly shows that at energies below the threshold, the populations closely maintain a 445 K Boltzmann profile during reaction. In contrast, the energy level populations near and above threshold are significantly depleted due to the efficient unimolecular decomposition. This general scenario is characteristic of the low-pressure limit.

Goeringer and McLuckey²⁸ modeled the collisional relaxation of internally excited high mass ions (> 1 kDa) held in a quadrupole ion trap. They simulated the energy transfer with both a random walk model based on an exponential model with small steps, and with a diffusion model that assumed that the He atom and the ion thermally equilibrated during the collision. They predict that polypeptide ions cool from 450 to 300 K in less than 10 ms in 1 mTorr of He. The results from the present study support their more efficient energy transfer model.

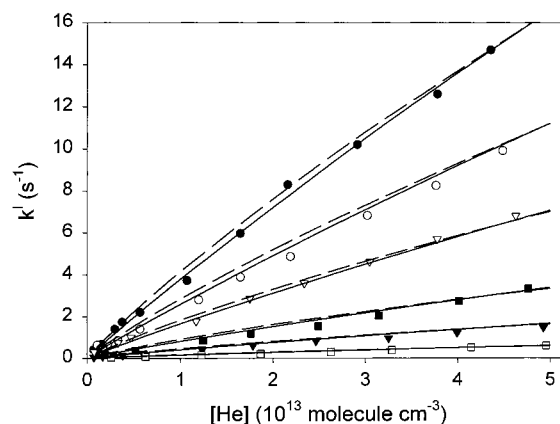


Figure 9. $\text{H}^+(\text{CH}_3\text{CN})_2$ first-order decomposition rate coefficients vs $[\text{He}]$ and temperature. Solid lines are master equation calculations for $E_0 = 29.5$ kcal mol^{-1} , $\beta = 1.55$ kcal mol^{-1} , and the orbiting limit decomposition rate constants. The dashed lines are for $E_0 = 28.7$ kcal mol^{-1} and $\beta = 1.54$ kcal mol^{-1} with one tenth the orbiting limit decomposition rate coefficients. The temperatures are 487, 513, 534, 559, 577, and 594 K (bottom to top).

The calculated second-order rate coefficients for thermal decomposition of $\text{H}^+(\text{H}_2\text{O})_3$ varied by less than 2% when the number of energy increments in the master equation calculation was increased from 100 to 200 (energy increments of 0.28 and 0.14 kcal mol^{-1} , respectively). The best fit $\text{H}^+(\text{H}_2\text{O})_3$ bond energy was somewhat sensitive to the factor used to scale the ab initio vibrational frequencies of the reactant and products. The best-fit bond energies varied as 20.0, 19.8, and 19.2 for scale factors of 0.79, 0.89, and 1.0, respectively. The corresponding best-fit average energy up β was relatively insensitive to the vibrational scale factor, increasing from 1.1 to 1.2 for scale factors of 0.79 and 1.0, respectively.

In the previous study of the calibration clusters,⁷ linear fits to the first-order decomposition rate coefficients vs $[\text{He}]$ plots had small positive intercepts. The data for $\text{H}^+(\text{CH}_3\text{CN})_2$ and $\text{H}^+(\text{C}_2\text{H}_5\text{OH})_2$ had the largest intercepts. The $\text{H}^+(\text{CH}_3\text{CN})_2$ measurements were repeated in the present work with an extended $[\text{He}]$ range to better resolve possible curvature that may have contributed to the intercepts. The new experimental data and master equation calculations are shown in Figure 9. The new results are slightly curved and do go through the origin. The curvature is reproduced by the master equation model, and the second-order rate coefficients and activation energy agree well with the previous measurements.⁷ Linear fits of the new k^1 data (Figure 9) over a range of $[\text{He}]$ similar to that used in the previous study give significant positive intercepts, e.g., 0.7 s^{-1} at the highest temperature. These are comparable to the intercepts observed in the previous study.

The new $\text{H}^+(\text{CH}_3\text{CN})_2$ data were also fit with the master equation model using decomposition rate coefficients that were 10 times smaller than the orbiting limit to test the sensitivity of the overall kinetics to the unimolecular rate constants k_{uni} . The results are plotted as dashed lines in Figure 9. Smaller unimolecular rate coefficients increase the curvature in k^1 vs $[\text{He}]$ because they shift the overall kinetics away from the low-pressure limit toward the fall-off region. The temperature dependence is reproduced well, even with the reduced decomposition rate constants. However, the bond energy required to fit the data is 1 kcal mol^{-1} smaller when the reduced decomposition rate constants are employed. The $\text{H}^+(\text{CH}_3\text{CN})_2$ kinetics are fit best with the full orbiting decomposition rate coefficients, but rate coefficients as small as 0.1 times the orbiting limit probably cannot be ruled out.

TABLE 2: $\text{HSO}_4^-(\text{H}_2\text{SO}_4)_x(\text{HNO}_3)_y$ Measurement Conditions and Master Equation Results^a

reaction	T_{avg} (K)	$E_a(T_{\text{avg}})^b$ (kcal mol ⁻¹)	$U_{\text{vib}}(T_{\text{avg}})^c$ (kcal mol ⁻¹)	E_o^d (kcal mol ⁻¹)	β^e (kcal mol ⁻¹)	$\Delta H^\circ_{298\text{K}}$ (kcal mol ⁻¹)
$\text{HSO}_4^-\text{H}_2\text{SO}_4 \rightarrow \text{HSO}_4^- + \text{H}_2\text{SO}_4$	576	26.5	15.5	41.2	2.00	41.8
$\text{HSO}_4^-(\text{H}_2\text{SO}_4)_2 \rightarrow \text{HSO}_4^-\text{H}_2\text{SO}_4 + \text{H}_2\text{SO}_4$	434	10.8	16.8	27.6	1.29	27.4
$\text{HSO}_4^-(\text{H}_2\text{SO}_4)_3 \rightarrow \text{HSO}_4^-(\text{H}_2\text{SO}_4)_2 + \text{H}_2\text{SO}_4$	348	11.3	16.6	24.0	0.88	23.8
$\text{HSO}_4^-(\text{H}_2\text{SO}_4)_4 \rightarrow \text{HSO}_4^-(\text{H}_2\text{SO}_4)_3 + \text{H}_2\text{SO}_4$	324	9.0	19.3	21.8	0.74	21.6
$\text{HSO}_4^-(\text{H}_2\text{SO}_4)_5 \rightarrow \text{HSO}_4^-(\text{H}_2\text{SO}_4)_4 + \text{H}_2\text{SO}_4$	319	5.8	23.2	20.5	0.68	20.4
$\text{HSO}_4^-\text{HNO}_3 \rightarrow \text{HSO}_4^- + \text{HNO}_3$	478	16.7	9.4	27.4	1.59	27.4
$\text{HSO}_4^-(\text{HNO}_3)_2 \rightarrow \text{HSO}_4^-\text{HNO}_3 + \text{HNO}_3$	323	8.5	8.4	17.5	1.00	17.0
$\text{HSO}_4^-\text{H}_2\text{SO}_4\text{HNO}_3 \rightarrow \text{HSO}_4^-\text{H}_2\text{SO}_4 + \text{HNO}_3$	323	7.4	9.1	16.7	0.67	16.1

^a Molecular parameters for the most stable ab initio structures⁹ were used in the master equation calculations. ^b Activation energy derived from low pressure ($[\text{He}] < 5 \times 10^{12}$ molecule cm⁻³) kinetics. ^c Vibrational energy of reactant ion. ^d Best fit bond energy derived from the master equation calculations. ^e Best fit energy transfer parameter derived from the master equation calculations.

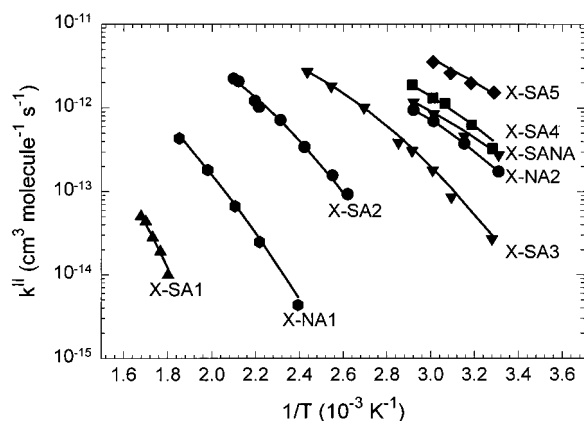


Figure 10. Arrhenius plots for decomposition of $\text{HSO}_4^-(\text{H}_2\text{SO}_4)_x(\text{HNO}_3)_y$. The points are experimental data and the lines were calculated with the master equation analysis and parameters listed in Table 2. Nomenclature is as follows: X- = HSO_4^- , SA = H_2SO_4 , NA = HNO_3 , i.e., X-SANA = $\text{HSO}_4^-\text{H}_2\text{SO}_4\text{HNO}_3$.

Master Equation Calculations for $\text{HSO}_4^-(\text{H}_2\text{SO}_4)_x(\text{HNO}_3)_y$. The decomposition kinetics of $\text{HSO}_4^-(\text{H}_2\text{SO}_4)_{1,2}$, $\text{HSO}_4^-(\text{HNO}_3)_{1,2}$, and $\text{HSO}_4^-\text{H}_2\text{SO}_4\text{HNO}_3$ are in or near the low pressure limit, similar to the calibration clusters described above. These kinetics are characterized by linear or only slightly curved k^I vs $[\text{He}]$ data and adherence to the simple relationship $E_o = U_{\text{vib}} + E_a + 1.2k_B T$. The larger sulfuric clusters, $\text{HSO}_4^-(\text{H}_2\text{SO}_4)_{3,4,5}$ have kinetics in the fall-off regime with curved k^I vs $[\text{He}]$ plots, and optimized master equation bond energies that are considerably smaller than predicted by $E_o = U_{\text{vib}} + E_a + 1.2k_B T$. The temperature dependencies of the second-order decomposition rate constants are plotted in Figure 10. For the $\text{HSO}_4^-(\text{H}_2\text{SO}_4)_{3,4,5}$ clusters, that have kinetics in the fall-off regime, the second order rate coefficients were derived from linear fits to the lowest pressure data, typically with $[\text{He}] < 5 \times 10^{12}$ molecule cm⁻³. Note that even at these low pressures the kinetics are not in the low-pressure limit. This analysis is used because the Arrhenius plot is a useful way to visualize the temperature dependence of the data. The solid lines in Figure 10 are the master equation thermal decomposition rate coefficients calculated using the parameters listed in Table 2. Samples of the pressure dependencies of the first-order decomposition rate coefficients for $\text{HSO}_4^-(\text{H}_2\text{SO}_4)_{2-5}$ cluster ions in the fall-off region are shown in Figure 11 along with the master

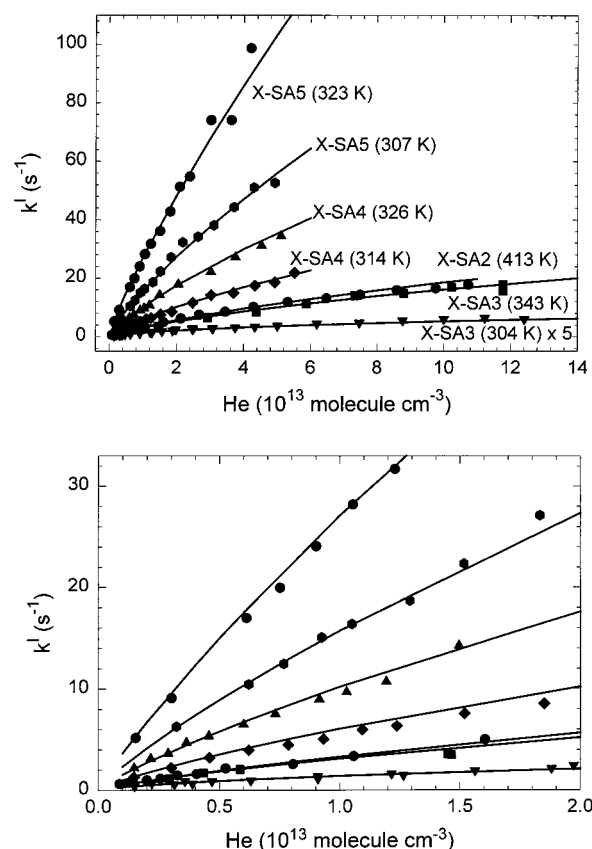


Figure 11. First-order rate coefficients for decomposition of $\text{HSO}_4^-(\text{H}_2\text{SO}_4)_{2,3,4,5}$ as a function of $[\text{He}]$ and temperature. The low-pressure portion of the data in (a) is expanded in (b). Lines are master equation results for the parameters listed in Table 2. The nomenclature is the same as used in Figure 10.

equation model results. The master equation model reproduces both the pressure and temperature dependencies. The modeled temporal evolution of the energy level distributions of $\text{HSO}_4^-(\text{H}_2\text{SO}_4)_4$ at 314 K with $[\text{He}] = 3 \times 10^{13}$ molecule cm⁻³ is shown in Figure 12. The simulation was initiated with a 300 K Boltzmann distribution to avoid large immediate ion losses that would have been observed with higher starting temperatures. As discussed above, the steady-state decomposition kinetics are independent of the starting distribution. Similar to $\text{H}^+(\text{H}_2\text{O})_3$ (Figures 6 and 7), the $\text{HSO}_4^-(\text{H}_2\text{SO}_4)_4$ populations of the energy

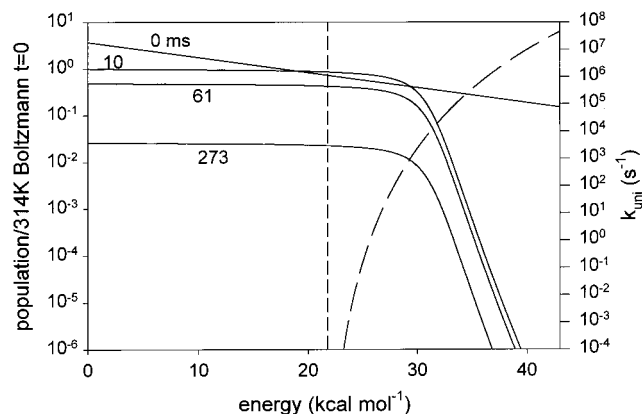


Figure 12. Calculated decomposition rate constants and temporal evolution of energy distributions for $\text{HSO}_4^-(\text{H}_2\text{SO}_4)_4$. The solid lines are the energy distributions plotted as the ratio to a 314 K Boltzmann distribution at $t = 0$, for a series of reaction times. The initial distribution is a 300 K Boltzmann. The dashed vertical line marks the reaction threshold. The dashed curve is $k_{\text{uni}}(E)$. Master equation parameters are $E_0 = 21.8 \text{ kcal mol}^{-1}$, $\beta = 0.74 \text{ kcal mol}^{-1}$, $[\text{He}] = 3 \times 10^{13} \text{ molecule cm}^{-3}$, and $T = 314 \text{ K}$.

levels below threshold rapidly reach a steady state that resembles the ambient Boltzmann distribution. In contrast to $\text{H}^+(\text{H}_2\text{O})_3$, the $\text{HSO}_4^-(\text{H}_2\text{SO}_4)_4$ unimolecular decomposition is slow relative to the energy transfer at the reaction threshold, and at steady state there is significant population of states up to about 30 kcal mol^{-1} , roughly 8 kcal mol^{-1} above the reaction threshold. The slow decomposition kinetics at threshold are due to the high reactant state density ($\rho(E_0) = 1 \times 10^{30} \text{ states kcal}^{-1} \text{ mol}$; $(\hbar\rho(E_0))^{-1} = 1 \times 10^{-17} \text{ s}^{-1}$). Above about 30 kcal mol^{-1} there is significant depletion of population relative to the Boltzmann distribution because unimolecular decomposition competes effectively with energy transfer. This scenario, where there is some steady-state population above threshold, but not a complete Boltzmann distribution, is characteristic of systems in the fall-off region. It is interesting to note that at the pressures examined in the present work ($[\text{He}] > 1 \times 10^{12} \text{ molecule cm}^{-3}$) the $\text{HSO}_4^-(\text{H}_2\text{SO}_4)_4$ decomposition kinetics are far removed from the low-pressure limit. Low-pressure limit kinetics obtain when decomposition at threshold is more efficient than energy transfer. For $\text{HSO}_4^-(\text{H}_2\text{SO}_4)_4$ the unimolecular decomposition at threshold ($k_{\text{uni}}(E_0) \approx 10^{-7} \text{ s}^{-1}$) is comparable to the He collision frequency when $[\text{He}] \approx 200 \text{ molecule cm}^{-3}$.

The slow decomposition of $\text{HSO}_4^-(\text{H}_2\text{SO}_4)_4$ at threshold E_0 relative to energy transfer shifts the effective reaction threshold from the bond energy $E_0 = 22 \text{ kcal mol}^{-1}$ to about 30 kcal mol^{-1} in 1 mTorr of He. In this case, the simple relationship given by Tolman's theorem can be expressed as $E_t = E_a + U_{\text{vib}} + ak_{\text{B}}T$, where E_t is the effective reaction threshold. Using $a = 1.2$, as with the calibration clusters,⁷ a value of $E_t = 29.4 \text{ kcal mol}^{-1}$ is derived for $\text{HSO}_4^-(\text{H}_2\text{SO}_4)_4$ ($U_{\text{vib}} = 19.3 \text{ kcal mol}^{-1}$, $E_a = 9.0 \text{ kcal mol}^{-1}$, $T = 324 \text{ K}$), consistent with Figure 12. This suggests that the bond energy may be extracted from measurements of the decomposition activation energy for systems in the fall-off region by applying Tolman's theorem, if the unimolecular rate coefficients can be calculated.

Comparison of Energy Transfer Probabilities with Ergodic Collision Theory. The ergodic collision theory (ECT) described by Nordholm et al.²⁹ provides a useful benchmark for comparison of the energy transfer probabilities. Ergodic collision theory yields energy transfer probabilities for the limit of statistical energy transfer. In the present work, ECT probabilities were calculated using the expressions of Nordholm et al.,²⁹ with cluster ion densities of states calculated from direct

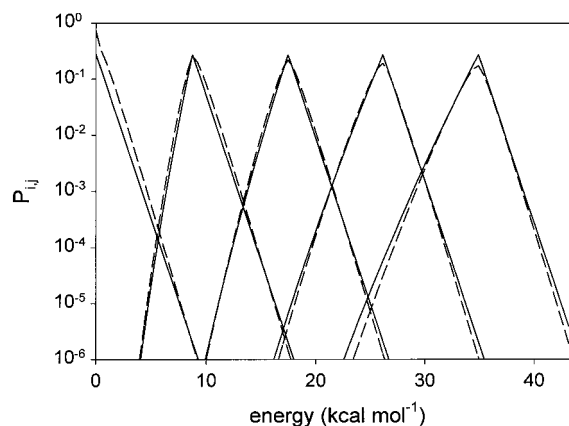


Figure 13. Energy transfer probabilities for $\text{HSO}_4^-(\text{H}_2\text{SO}_4)_4$ calculated with ergodic collision theory (dashed lines) and the exponential up model (solid lines) with optimized parameters (Table 2) at 326 K. The energy level spacing is $0.44 \text{ kcal mol}^{-1}$.

state counts. ECT probabilities for $\text{H}^+(\text{H}_2\text{O})_3$ are plotted in Figure 3 along with the probabilities for the best fit exponential up model at 445 K. Average energies transferred (eqs 5, 6, and 7) are plotted in Figure 4. It is interesting that ergodic collision theory predicts average energies up that are comparable to those found in the present work, and that are also independent of the internal energy of the ion. However, the optimized exponential up model gives more efficient downward energy transfer, with average energies down about 50% larger than the ECT results. The $\text{H}^+(\text{H}_2\text{O})_3$ kinetic data set could not be fit employing the ECT energy transfer probabilities. The second-order $\text{H}^+(\text{H}_2\text{O})_3$ decomposition rate coefficient at 445 K is reproduced with a master equation calculation using ECT energy transfer probabilities and $E_0 = 19.5 \text{ kcal mol}^{-1}$, which is comparable to the best fit value employing the exponential up model ($19.8 \text{ kcal mol}^{-1}$), but the ECT based master equation calculation overestimates the activation energy ($E_a = 13.5 \text{ kcal mol}^{-1}$ vs the experimental value of $11.9 \text{ kcal mol}^{-1}$).

In contrast to $\text{H}^+(\text{H}_2\text{O})_3$, the $\text{HSO}_4^-(\text{H}_2\text{SO}_4)_4$ decomposition kinetics are reproduced very well with a master equation calculation based on ECT energy transfer probabilities. The optimized bond energy for the ECT based calculation is $22.0 \text{ kcal mol}^{-1}$ which is similar to the best-fit value derived with the exponential up model ($E_0 = 21.8 \text{ kcal mol}^{-1}$). ECT energy transfer probabilities for $\text{HSO}_4^-(\text{H}_2\text{SO}_4)_4$ are similar to the probabilities from the exponential up model (Figure 13). The average energy up for the ECT probabilities at 326 K is about $0.8 \text{ kcal mol}^{-1}$ (Figure 14) and independent of internal energy ($0\text{--}35 \text{ kcal mol}^{-1}$). This is close to the value required to fit the kinetics using the exponential up energy transfer model ($\beta = 0.74 \text{ kcal mol}^{-1}$). ECT net and down average energies transferred are also very similar to the best-fit exponential up results (Figure 14).

The optimized average energies up β for the exponential up model (Table 1) are plotted vs average reaction temperature for all of the cluster ions in Figure 15. Note that in the master equation model, β for each cluster is a constant, and does not vary with reaction temperature. The average energies up are correlated with the average reaction temperature, and a least-squares fit forced through the origin gives $\beta = 1.6k_{\text{B}}T$. Average energies up for the ECT energy transfer probabilities at the average temperatures are also plotted in Figure 15. Despite a wide variety of state densities, all of the ECT average energies up fall closely on a line given by $1.24k_{\text{B}}T$. The ECT average energies up for the individual clusters also vary with temperature roughly as $1.2k_{\text{B}}T$. However, fitting the decomposition kinetics

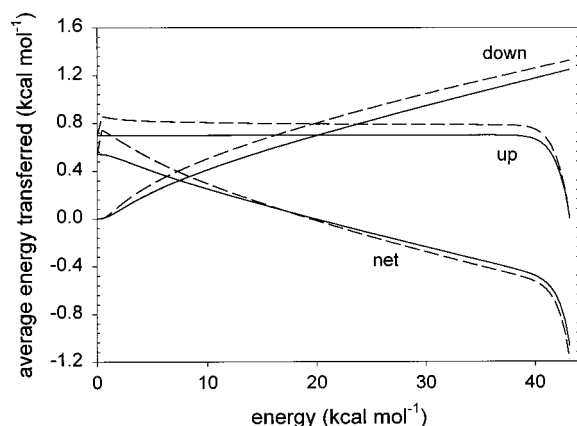


Figure 14. Average energy transfer for the probabilities in Figure 13. Solid lines are for the exponential model and dashed lines are for ergodic collision theory.

for several of the calibration clusters ($\text{H}^+(\text{H}_2\text{O})_3$, $\text{H}^+(\text{H}_2\text{O})_4$, and $\text{H}^+(\text{C}_2\text{H}_5\text{OH})_2$) using $\beta = ck_{\text{B}}T$ with c as a variable, yields bond energies that are systematically lower than the literature values by 2 kcal mol⁻¹. Interestingly, even though the bond energies are probably too small, the best-fit values of c are all in the range 1.0 ± 0.2 , consistent with ergodic collision theory.

In general, the cluster ion-He energy transfer appears to be similar to the statistical limit given by ergodic collision theory. This contrasts the situation for energy transfer between neutral collision partners, where typically the average energy transferred is less than 10% of the statistical limit.³⁰ The efficient energy transfer in ion-molecule systems is consistent with the strong electrostatic interaction between the ion and the bath gas that leads to long-lived collision complexes.

Comparison with Previous Studies of Ion-Molecule Energy Transfer. Efficient ion-molecule energy transfer has also been reported by Marzluff et al.³¹ who studied the collision-induced decomposition of deprotonated peptides in an ion cyclotron mass spectrometer. From measured decomposition kinetics, they estimated that roughly 50% of the 1.25 eV collision energy is transferred in collisions between N_2 and glygly ile. They also performed trajectory calculations for the same system that yielded comparable efficiencies.

Meroueh and Hase³² calculated classical trajectories for the collisional activation of peptide ions. They reported that 40% to 75% of the collision energy (20–1000 kcal mol⁻¹) is transferred to the ion in head on collisions. They noted that the efficiencies at low energy are consistent with a statistical model.

Collisional deactivation of excited ions has been studied by direct laser excitation and with measurements of the kinetics of termolecular reactions. Barfknecht and Brauman³³ reported that He removes about 0.3 kcal mol⁻¹ per collision from highly excited bromo-3-(trifluoromethyl)-benzene ion prepared with an internal energy of 55 kcal mol⁻¹. Ahmed and Dunbar³⁴ measured the collisional relaxation of benzene ions with the technique of chopped laser two photon photodissociation. They reported net energy removal per collision of about 0.3 kcal mol⁻¹ for an ion internal energy of 59 kcal mol⁻¹ and a helium collision partner. This value is slightly lower than the net energy removal they measured for bromobenzene ions (0.7 kcal mol⁻¹).³⁵

Cates and Bowers³⁶ reported collision stabilization efficiencies for excited $\text{H}^+(\text{CH}_3)_3\text{N}_2$ based on measurements of the kinetics for the association reaction $(\text{CH}_3)_3\text{NH}^+ + (\text{CH}_3)_3\text{N} + \text{M} \rightarrow \text{H}^+(\text{CH}_3)_3\text{N}_2 + \text{M}$ at low pressure. They measured efficiencies for $\text{M}=\text{He}$, defined as the ratio of the quenching rate constant

for He to the quenching rate constant for $(\text{CH}_3)_3\text{N}$, of about 0.3. It is difficult to extract the average energy transferred per collision from this number without detailed modeling. Chang and Golden³⁷ have also analyzed low-pressure association kinetics, and derived weak collision efficiencies, defined as the ratio of the observed decomposition rate constant to the strong collision rate constant. The strong collision rate constant is the low-pressure limit rate constant calculated by assuming that the reactant maintains a Boltzmann distribution and that each collision of the bath gas with molecules having energies above the threshold energy leads to reaction. Chang and Golden concluded that for small complexes the collision efficiency is close to unity (strong collisions), and for larger complexes e.g., $(\text{C}_6\text{H}_6)^+_2$ the collision efficiencies for Helium are on the order of 0.01. These numbers are somewhat smaller than the He collision efficiencies (0.1–1) measured for the calibration cluster ions⁷ reexamined in the present work.

Gilbert and McEwan³⁸ modeled the pressure dependence of the termolecular association reaction $\text{CH}_3^+ + \text{HCN} + \text{He} \rightarrow \text{C}_2\text{H}_4\text{N}^+ + \text{He}$ with a master equation analysis based on RRKM theory and parametrized energy transfer probabilities. They concluded that the average energy transferred down is about 2 kcal mol⁻¹ for the excited CH_3NCH^+ complex. Smith et al.³⁹ reexamined this system with an angular momentum conserved master equation analysis and concluded that the average rotational and internal energy transferred down are both about 0.4 kcal mol⁻¹.

It is difficult to make direct comparisons between the energy transfer results of the present study and previous work because the ions and the conditions are different. The results of the present study suggest that the average energy up is a function of temperature and roughly independent of the nature of the ion and the ion internal energy, at least for relatively large cluster ions. The net average energy transfer, which is probed in the direct excitation experiments and via association kinetics, is a function of the nature of the ion, the ion energy, and the temperature. For $\text{H}^+(\text{H}_2\text{O})_3$ and $\text{HSO}_4^-(\text{H}_2\text{SO}_4)_4$ (Figures 4 and 14), the present work suggests that the net average energies transferred per collision are e.g., -3 and -0.4 kcal mol⁻¹ for internal energies of 25 and 40 kcal mol⁻¹, respectively. These numbers are comparable to the results listed above from previous studies of other ions. The general conclusions from the previous studies^{31,32} that energy transfer to large bio-ions is efficient, is entirely consistent with the conclusions of the present study.

$\text{HSO}_4^-(\text{H}_2\text{SO}_4)_x(\text{HNO}_3)_y$ Bond Enthalpies. Bond enthalpies at 298 K for the $\text{HSO}_4^-(\text{H}_2\text{SO}_4)_x(\text{HNO}_3)_y$ clusters are listed in Table 2. The bond enthalpies were calculated from the bond energies by using standard formulas⁴⁰ with the scaled ab initio harmonic vibrational frequencies.⁹ The nitric acid bond energies are in good agreement (± 0.7 kcal mol⁻¹) with those derived in the previous paper⁹ using the simple expression $E_o = U_{\text{vib}} + E_a + 1.2k_{\text{B}}T$. The $\text{HSO}_4^-\text{H}_2\text{SO}_4$ bond enthalpy is in reasonable agreement with Evleth's MP2/6-31+G* ab initio value of 47 kcal mol⁻¹⁴¹ and his estimated lower limit of 40 kcal mol⁻¹. $\text{HSO}_4^-\text{H}_2\text{SO}_4$ is unusually strongly bound, consistent with its ability to form three favorable hydrogen bonds.^{9,41} Arnold and co-workers^{42–44} have reported estimates for bond enthalpies of some $\text{HSO}_4^-(\text{H}_2\text{SO}_4)_x(\text{HNO}_3)_y$ clusters based on atmospheric ion measurements. They converted cluster ion signal intensities to Gibbs free energy changes for the clustering reactions by assuming that the ions were in equilibrium and deriving the gas-phase concentrations of H_2SO_4 and HNO_3 from the ion distributions. Qiu and Arnold⁴⁴ extended this type of analysis, and derived ΔH° and ΔS° from the change in the Gibbs free

TABLE 3: Summary of $\text{HSO}_4^-(\text{H}_2\text{SO}_4)_x(\text{HNO}_3)_y$ Bond Enthalpies Derived from Atmospheric Ion Measurements

reaction	ΔG°_T (kcal mol ⁻¹)	<i>T</i> (K)	ref	$\Delta S^\circ_{298\text{K}}^a$ (cal mol ⁻¹ K ⁻¹)	ΔH°^b (kcal mol ⁻¹)
$\text{HSO}_4^-(\text{H}_2\text{SO}_4)_2 \rightarrow$ $\text{HSO}_4^- + \text{H}_2\text{SO}_4 + \text{H}_2\text{SO}_4$	> 15.8	250	ref 42	35.8	> 24.8
$\text{HSO}_4^-(\text{H}_2\text{SO}_4)_3 \rightarrow$ $\text{HSO}_4^- + (\text{H}_2\text{SO}_4)_2 + \text{H}_2\text{SO}_4$	14	233	ref 43	36.7	22.6
	14.6	250	ref 42		23.8
	14.7	246	ref 44		23.7
$\text{HSO}_4^-(\text{H}_2\text{SO}_4)_4 \rightarrow$ $\text{HSO}_4^- + (\text{H}_2\text{SO}_4)_3 + \text{H}_2\text{SO}_4$	13	233	ref 43	37.1	21.6
	13	246	ref 44		22.1
$\text{HSO}_4^-(\text{H}_2\text{SO}_4)_5 \rightarrow$ $\text{HSO}_4^- + (\text{H}_2\text{SO}_4)_4 + \text{H}_2\text{SO}_4$	13	233	ref 43	36.2	21.4
$\text{HSO}_4^-(\text{HNO}_3)_2 \rightarrow$ $\text{HSO}_4^- + (\text{HNO}_3) + \text{HNO}_3$	11.2	233	ref 43	26.5	17.4

^a Calculated from the ab initio entropies reported in the previous paper (ref 9). ^b $\Delta H^\circ = \Delta G^\circ + T\Delta S^\circ$.

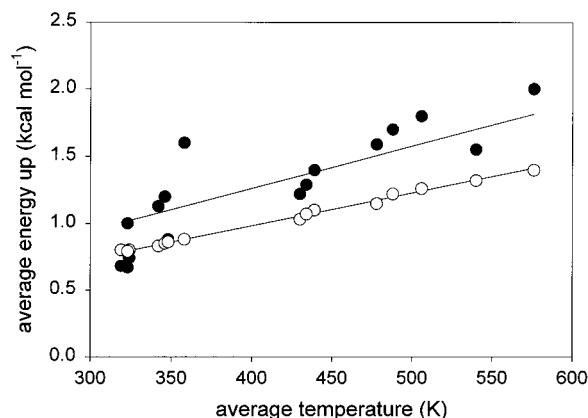


Figure 15. Temperature dependence of the average energy up for the calibration clusters and the $\text{HSO}_4^-(\text{H}_2\text{SO}_4)_x(\text{HNO}_3)_y$ clusters. Solid circles are for the exponential up model (average energy up = β , Tables 1 and 2). Open circles are the average energies up from ergodic collision theory. The lines are fits forced through the origin giving $\beta = 1.59k_B T$ for the exponential up results (solid circles) and $\beta = 1.24k_B T$ for the ECT results (open circles).

energy as a function of temperature, by analyzing data from different altitudes. However, due to the limited temperature range (239–253 K), the derived parameters are likely to be highly uncertain. A third law analysis is probably more appropriate, where the entropy change is fixed and the enthalpy change is derived. Bond enthalpies determined from the atmospheric ion distributions by using the entropies reported in paper (I) and the Gibbs free energy changes from the atmospheric measurements are listed in Table 3. These values are in good agreement with those measured in the present work. The bond energies derived in the present work are also within 3 kcal mol⁻¹ of the HF/6-31+G(d) ab initio values reported in paper (I).

The $\text{HSO}_4^-(\text{H}_2\text{SO}_4)_x$ bond enthalpies decrease monotonically with the number of H_2SO_4 ligands, similar to most other ion–molecule systems.⁴⁵ The bond enthalpy approaches within 10% of the H_2SO_4 enthalpy of vaporization ($\Delta H_{v,298\text{K}} = 18.8$ kcal mol⁻¹)⁴⁰ by $x = 5$ ligands.

Summary

Measurements of the kinetics of thermal decomposition of cluster ions in a quadrupole ion trap were analyzed with a master equation model. The model, which is based on exponential up energy transfer and an orbiting transition state, reproduced the pressure and temperature dependence of the decomposition kinetics for a set of calibration clusters in the low-pressure limit. Input to the model included vibrational frequencies and rotational constants for the reactants and products calculated ab initio

at the HF/6-31+G(d) level. Direct harmonic state counts were employed. Variable parameters included the bond energy and the average energy transferred in up collisions. The best-fit bond energies from the master equation model reproduced the literature bond energies to better than 1 kcal mol⁻¹. The helium-cluster ion energy transfer is very efficient, resembling the predictions of ergodic collision theory, with average energies up ranging from about 0.5 to 2 kcal mol⁻¹ per collision. The master equation analysis was extended to derive bond energies for cluster ions of the form $\text{HSO}_4^-(\text{H}_2\text{SO}_4)_x(\text{HNO}_3)_y$, some of which have kinetics in the fall-off region. The $\text{HSO}_4^-(\text{H}_2\text{SO}_4)_x$ – $(\text{HNO}_3)_y$ bond energies are important for understanding the chemical composition of atmospheric cluster ions, and for the prediction of ion induced nucleation rates.

Acknowledgment. The authors are grateful to Harald Stark, Karl Froyd, Sean Smith, and Roberto Bianco for useful discussions. This work was performed while J.C. held a National Research Council Research Associateship Award at the NOAA Aeronomy Lab. This work was supported in part by NOAA's Climate and Global Change Program.

References and Notes

- (1) Tardy, D. C.; Rabinovitch, B. S. *Chem. Rev.* **1977**, *77*, 369.
- (2) Quack, M.; Troe, J. *Gas Kinetics and Energy Transfer*; The Chemical Society: London, 1977; vol. 2.
- (3) Flynn, G. W. *Acc. Chem. Res.* **1981**, *14*, 334.
- (4) Oref, I.; Tardy, D. C. *Chem. Rev.* **1990**, *90*, 1407.
- (5) Flynn, G. W.; Parmenter, C. S.; Wodtke, A. M. *J. Phys. Chem.* **1996**, *100*, 12817.
- (6) Armentrout, P. B.; Baer, T. *J. Phys. Chem.* **1996**, *100*, 18 266.
- (7) Lovejoy, E. R.; Bianco, R. *J. Phys. Chem.* **2000**, *104*, 10 280.
- (8) Tolman, R. C. *J. Am. Chem. Soc.* **1920**, *42*, 2506. Dunbar, R. C. *J. Phys. Chem.* **1994**, *98*, 8705. Dunbar, R. C. *J. Chem. Phys.* **1991**, *95*, 2537.
- (9) Curtius, J.; Froyd, K. D.; Lovejoy, E. R., *J. Phys. Chem. A* **2001**, 10867.
- (10) see e.g. Troe, J. *J. Chem. Phys.* **1977**, *66*, 4745. Gaynor, B. J.; Gilbert, R. G.; King, K. D. *Chem. Phys. Lett.* **1978**, *55*, 40. Gilbert, R. G.; Luther, K.; Troe, J. *Ber. Bunsen-Ges. Phys. Chem.* **1983**, *87*, 169.
- (11) Su, T.; Bowers, M. T. *Classical Ion–Molecule Collision Theory. Gas-Phase Ion Chemistry*; Bowers, M. T., Ed.; Academic Press: New York, 1979; vol. 1.
- (12) Press, W. H.; Teukolsky, S. A.; Vetterling, W. T.; Flannery, B. T. *Numerical Recipes in Fortran 77: The Art of Scientific Computing*; Cambridge University Press: 1992.
- (13) see e.g., Snider, N. *J. Phys. Chem.* **1986**, *90*, 4366.
- (14) Lenzer, T.; Luther, K.; Troe, J.; Gilbert, R. G.; Lim, K. F. *J. Chem. Phys.* **1995**, *103*, 626. Barker, J. R. *Ber. Bunsen-Ges. Phys. Chem.* **1997**, *101*, 566. Lenzer, T.; Luther, K.; Reihs, K.; Symonds, A. C. *J. Chem. Phys.* **2000**, *112*, 4090.
- (15) Gilbert, R. G.; King, K. D. *Chem. Phys.* **1980**, *49*, 367.
- (16) Chesnavich, W. T.; Bowers, M. T. *Statistical Methods in Reaction Dynamics. Gas-Phase Ion Chemistry*; Bowers, M. T., Ed.; Academic Press: New York, 1979; vol. 1.
- (17) Olzmann, M.; Troe, J. *Ber. Bunsen-Ges. Phys. Chem.* **1992**, *96*, 1327.
- (18) Chesnavich, W. J.; Bowers, M. T. *J. Chem. Phys.* **1977**, *66*, 2306.
- (19) Bass, L. M.; Bowers, M. T. *J. Chem. Phys.* **1987**, *86*, 2611.

- (20) Su, T.; Chesnavich J. *Chem. Phys.* **1982**, 76, 5183.
- (21) CRC *Handbook of Chemistry and Physics*, 70th ed.; Weast, R. C., Ed.; CRC press: Boca Raton, 1989.
- (22) Kuczkowski, R. L.; Suenram, R. D.; Lovas, F. J. *J. Am. Chem. Soc.* **1981**, 103, 2561.
- (23) Lippincott, E. R.; Nagarajan, G.; Stutman, J. M. *J. Phys. Chem.* **1966**, 70, 78.
- (24) Beyer, T.; Swinehart, D. R. *ACM Commun.* **1973**, 16, 379. Stein, S. F.; Rabinovitch, B. S. *J. Chem. Phys.* **1973**, 58, 2438.
- (25) Scott, A. P.; Radom, L. *J. Phys. Chem.* **1996**, 100, 16 502.
- (26) see e.g. Nakashima, N.; Yoshihara, K. *J. Chem. Phys.* **1983**, 79, 2727. Dove, J. E.; Hippler, H.; Troe, J. *J. Chem. Phys.* **1985**, 82, 1907. Zellweger, J.-M.; Brown, T. C.; Barker, J. R. *J. Phys. Chem.* **1986**, 90, 461. Wright, S. M. A.; Sims, I. R.; Smith, I. W. M. *J. Phys. Chem. A* **2000**, 104, 10 347.
- (27) Lenzer, T.; Luther, K.; Reihs, K.; Symonds, A. C. *J. Chem. Phys.* **2000**, 112, 4090.
- (28) Goeringer, D. E.; McLuckey, S. A. *Int. J. Mass Spec.* **1998**, 177, 163.
- (29) Nordholm, S.; Freasier, B. C.; Jolly, D. L. *Chem. Phys.* **1977**, 25, 433.
- (30) Börjesson, L. E. B.; Nordholm, S. *J. Phys. Chem.* **1995**, 99, 938.
- (31) Marzluff, E. M.; Campbell, S.; Rodgers, M. T.; Beauchamp, J. L. *J. Am. Chem. Soc.* **1994**, 116, 6947.
- (32) Meroueh, O.; Hase, W. L. *Int. J. Mass Spectrom.* **2000**, 201, 233.
- (33) Barfknecht, A. T.; Brauman, J. I. *J. Chem. Phys.* **1986**, 84, 3870.
- (34) Ahmed, M. S.; Dunbar, R. C. *J. Chem. Phys.* **1988**, 89, 4829.
- (35) Ahmed, M. S.; Dunbar, R. C. *J. Am. Chem. Soc.* **1987**, 109, 3215.
- (36) Cates, R. D.; Bowers, M. T. *J. Am. Chem. Soc.* **1980**, 102, 3994.
- (37) Chang, J. S.; Golden, D. M. *J. Am. Chem. Soc.* **1981**, 103, 496.
- (38) Gilbert, R. G.; McEwan, M. J. *Aust. J. Chem.* **1985**, 38, 231.
- (39) Smith, S. C.; McEwan, M. J.; Gilbert, R. G. *J. Chem. Phys.* **1989**, 90, 1630.
- (40) Chase, M. W., Jr.; Davies, C. A.; Downey, J. R., Jr.; Frurip, D. J.; McDonald, R. A.; Syverud, A. N. JANAF Thermochemical Tables. *J. Phys. Chem. Ref. Data Suppl. 1* **1985**, 14.
- (41) Evleth, E. M. *J. Mol. Struct. (THEOCHEM)* **1994**, 307, 179.
- (42) Arnold, F.; Qiu, S. *Planet. Space Sci.* **1984**, 32, 169.
- (43) Arnold, F.; Viggiano, A. A.; Schlager, H. *Nature, London* **1982**, 297, 371.
- (44) Qiu, S.; Arnold, F. *Chin. J. Space Sci.* **1985**, 5, 286.
- (45) Keese, R. G.; Castleman, A. W., Jr. *J. Phys. Chem. Ref. Data* **1986**, 15, 1011.
- (46) $\text{H}^+(\text{H}_2\text{O})_4$: Meot-ner, M.; Speller, C. V. *J. Phys. Chem.* **1986**, 90, 6616. Cunningham, A. J.; Payzant, J. D.; Kebarle, P. *J. Am. Chem. Soc.* **1972**, 94, 7672. Dalleska, N. F.; Honma, K.; Armentrout, P. B. *J. Am. Chem. Soc.* **1993**, 115, 12 125. Honma, K.; Sunderlin, L. S.; Armentrout, P. B. *J. Chem. Phys.* **1993**, 99, 1623. Meot-ner, M.; Field, F. H. *J. Am. Chem. Soc.* **1977**, 99, 998. Honma, K.; Sunderlin, L. S.; Armentrout, P. B. *Int. J. Mass Spectrom. Ion Proc.* **1992**, 117, 237. Lau, Y. K.; Ikuta, S.; Kebarle, P. *J. Am. Chem. Soc.* **1982**, 104, 1462. $\text{H}^+(\text{H}_2\text{O})_3$: Meot-ner, M.; Speller, C. V. *J. Phys. Chem.* **1986**, 90, 6616. Cunningham, A. J.; Payzant, J. D.; Kebarle, P. *J. Am. Chem. Soc.* **1972**, 94, 7672. Dalleska, N. F.; Honma, K.; Armentrout, P. B. *J. Am. Chem. Soc.* **1993**, 115, 12 125. Honma, K.; Sunderlin, L. S.; Armentrout, P. B. *J. Chem. Phys.* **1993**, 99, 1623. Meot-ner, M.; Field, F. H. *J. Am. Chem. Soc.* **1977**, 99, 998. Honma, K.; Sunderlin, L. S.; Armentrout, P. B. *Int. J. Mass Spectrom. Ion Proc.* **1992**, 117, 237. Hiraoka, K.; Takimoto, H.; Yamabe, S. *J. Phys. Chem.* **1986**, 90, 5910. $\text{H}^+(\text{CH}_3\text{OH})_3$: Grimsrud, E. P.; Kebarle, P. *J. Am. Chem. Soc.* **1973**, 95, 7939. Meot-ner, M. *J. Am. Chem. Soc.* **1992**, 114, 3312. $\text{H}^+(\text{C}_2\text{H}_5\text{OH})_2$: Larson, J. W.; McMahon, T. B. *J. Am. Chem. Soc.* **1982**, 104, 6255. Bomse, P. S.; Beauchamp, J. L. *J. Phys. Chem.* **1981**, 85, 488. $\text{H}^+(\text{CH}_3\text{CN})_2$: Meot-ner, M. *J. Am. Chem. Soc.* **1978**, 100, 4694. Speller, C. V.; Meot-ner, M. *J. Phys. Chem.* **1985**, 89, 5217. Honma, K.; Sunderlin, L. S.; Armentrout, P. B. *J. Chem. Phys.* **1993**, 99, 1623. $\text{H}^+(\text{CH}_3)_2\text{CO})_2$: Hiraoka, K.; Takimoto, H.; Yamabe, S. *J. Phys. Chem.* **1986**, 90, 5910. Larson, J. W.; McMahon, T. B. *J. Am. Chem. Soc.* **1982**, 104, 6255. Lau, Y. K.; Saluja, P. P. S.; Kebarle, P. *J. Am. Chem. Soc.* **1980**, 102, 7429. Szulejko, J. E.; McMahon, T. B. *Int. J. Mass Spec.* **1991**, 109, 279. Meot-ner, M.; Sieck, L. W. *J. Am. Chem. Soc.* **1991**, 113, 4448. $\text{NO}_3\text{-(HNO}_3)_2$: Davidson, J. A.; Fehsenfeld, F. C.; Howard, C. J. *Int. J. Chem. Kinet.* **1977**, 9, 17. Lee, N.; Keese, R. G.; Castleman, A. W., Jr. *J. Chem. Phys.* **1980**, 72, 1089. Wlodek, S.; Luczynski, Z.; Wincel, H. *Int. J. Mass Spectrom. Ion Phys.* **1980**, 35, 39. $\text{Cl}^-\text{H}_2\text{O}$: Hiraoka, K.; Mizuse, S.; Yamabe, S. *J. Phys. Chem.* **1988**, 92, 3943. Arshadi, M.; Yamdagni, R.; Kebarle, P. *J. Phys. Chem.* **1970**, 74, 1475. Sieck, L. W. *J. Phys. Chem.* **1985**, 89, 5552. Yamabe, S.; Furumiyu, Y.; Hiraoka, K.; Morise, K. *Chem. Phys. Lett.* **1986**, 131, 261. Larson, J. W.; McMahon, T. B. *J. Am. Chem. Soc.* **1984**, 106, 517. Burdett, N. A.; Hayhurst, A. N. *J. Chem. Soc., Faraday Trans. 1* **1982**, 78, 2997.